



ACADÉMIE
DES SCIENCES
INSTITUT DE FRANCE

Comptes Rendus

Mécanique


Thi Thu Hoai Bui, Thi Thu Huong Tran, Vu Nam Pham and Dinh Kien Nguyen

Large deflections of agglomerated carbon nanotubes reinforced sandwich cantilever beam partially embedded on foundation

Volume 353 (2025), p. 127-149

Online since: 9 January 2025

<https://doi.org/10.5802/crmeca.274>

 This article is licensed under the
CREATIVE COMMONS ATTRIBUTION 4.0 INTERNATIONAL LICENSE.
<http://creativecommons.org/licenses/by/4.0/>



*The Comptes Rendus. Mécanique are a member of the
Mersenne Center for open scientific publishing*
www.centre-mersenne.org — e-ISSN : 1873-7234



Research article / *Article de recherche*

Large deflections of agglomerated carbon nanotubes reinforced sandwich cantilever beam partially embedded on foundation

Grandes déflexions d'une poutre sandwich renforcée par des nanotubes de carbone agglomérés, partiellement encastrée sur une fondation

Thi Thu Hoai Bui ^{*,a,b}, Thi Thu Huong Tran ^c, Vu Nam Pham ^d and Dinh Kien Nguyen ^e

^a Graduate University of Science and Technology, VAST, 18 Hoang Quoc Viet, Hanoi, Vietnam

^b Faculty of Vehicle and Energy Engineering, Phenikaa University, Ha Dong, Hanoi 12116, Vietnam

^c School of Mechanical Engineering, Hanoi University of Science and Technology, Hanoi, Vietnam

^d Thuyloi University, 175 Son Tay, Dong Da, Hanoi, Vietnam

^e Institute of Mechanics, VAST, 18 Hoang Quoc Viet, Hanoi, Vietnam

E-mail: hoai.buithithu@phenikaa-uni.edu.vn (T. T. H. Bui)

Abstract. The large deflections of a carbon nanotubes (CNTs) reinforced sandwich cantilever beam partially embedded on Pasternak foundation are studied considering the influence of CNTs agglomeration. The sandwich beam is composed of a homogeneous core and composite face layers with effective moduli being estimated by Eshelby–Mori–Tanaka model. The nonlinear equilibrium equation is constructed using a first-order shear deformable nonlinear beam element and solved by the Newton–Raphson based iterative procedure. The result reveals that the effect of slenderness ratio on the large deflections is dependent on the degree of CNT agglomeration, and this effect is more significant when the agglomeration degree is more severe. The effects of the CNT volume fraction, the degree of CNTs agglomeration and the foundation parameters on the large deflections are studied in detail. The influence of the sandwich configuration and the porosities on the behavior of the sandwich beam is also examined and discussed.

Résumé. Les grandes déflexions d'une poutre sandwich renforcée par des nanotubes de carbone (CNTs) partiellement encastrée sur une fondation de Pasternak sont étudiées en tenant compte de l'influence de l'agglomération des CNTs. La poutre sandwich est composée d'un noyau homogène et de couches externes composites, dont les modules effectifs sont estimés à l'aide du modèle d'Eshelby–Mori–Tanaka.

L'équation d'équilibre non linéaire est construite en utilisant un élément de poutre non linéaire déformable en cisaillement de premier ordre, puis résolue à l'aide d'une procédure itérative basée sur l'algorithme de Newton–Raphson.

Les résultats révèlent que l'effet de l'élanement sur les grandes déflexions dépend du degré d'agglomération des CNTs, et cet effet devient plus important lorsque le degré d'agglomération est élevé. Les influences

*Corresponding author

de la fraction volumique des CNTs, du degré d'agglomération des CNTs et des paramètres de la fondation sur les grandes déflexions sont étudiées en détail. L'impact de la configuration sandwich et des porosités sur le comportement de la poutre sandwich est également examiné et discuté.

Keywords. Sandwich beam, Carbon nanotubes, Agglomeration, Partial foundation embedment, Large deflection.

Mots-clés. Poutre sandwich, Nanotubes de carbone, Agglomération, Encastrement partiel dans une fondation, Grande déflexion.

Funding. Vietnam National Foundation for Science and Technology Development (NAFOSTED) (grant number 107.02-2021.11).

Manuscript received 26 April 2024, revised 19 June 2024 and 28 September 2024, accepted 12 November 2024.

1. Introduction

Carbon nanotubes (CNTs), with low density but large surface area and high stiffness [1, 2], have made them a promising material for reinforcing polymer matrix. It was shown that the properties of polymer-based composites are significantly improved by using small amounts of CNTs as reinforcement [3, 4]. CNT-reinforced composite (CNTRC), therefore is an ideal material for fabricating high-performance structural elements. A large number of studies on the mechanical behavior of CNTRC structures are summarized in the review papers [5, 6], the investigations that are close to the present topic are discussed below.

Shen *et al.* [7, 8] employed the two-step perturbation technique to study the thermal effect of bending and buckling of CNTRC plates, in which the CNTs are graded in the thickness direction by different patterns. Shen and Xiang [9] proposed the multi-scale approach for studying nonlinear vibration, bending and post-buckling of functionally graded (FG) CNTRC beams embedded on foundation. Wattanasakulpong and Ungbhakorn [10] employed various beam theories to study vibration, bending and buckling of CNTRC beams, considering different types of CNT distribution. The effect of CNT gradation on behavior of beams made from FG-CNTRC was also considered by Mayandi *et al.* [11] using the finite element method. The Eshelby–Mori–Tanaka model was adopted by Lei *et al.* [12] to evaluate the properties of composite in their large deflection study of composite plates reinforced by CNTs. The large deformation and post-buckling of cylindrical panels made from CNT composite was studied in [13, 14] using the kp -Ritz method. The moving least square Ritz method was employed in [15–17] to study buckling and large deformation of CNTRC plates. Zghal *et al.* [18] developed a C^0 isoparametric shell element for studying large deformation of CNTRC plates and panels. The effect of CNT distributions on the nonlinear response of the CNTRC structures was numerically examined by the authors.

FG-CNTRC was also applied to sandwich structures to improve their performance. Bending and free vibration of sandwich plates with FG-CNTRC face layers were considered by Natarajan *et al.* [19] using an 8-node C^0 plate element. Their finding showed that the deflections are decreased by increasing the CNT volume, while the frequencies are increased. Buckling of Timoshenko beams and spherical caps made from sandwich CNT reinforced composite was considered in references [20, 21], considering the linear distribution of CNTs. The influence of the CNT volume fraction on the instability of CNTRC sandwich panels due to periodic loads was also examined in reference [22] using a Q8 plate element. Mehar *et al.* [23] used a higher-order finite element to assess stresses, deflections, and frequencies of sandwich plates with FG-CNTRC faces under thermo-mechanical loading. Thermal buckling of sandwich plates with CNTRC face sheets was studied by Kamarian [24] on the basis of a piecewise low-order shear deformation theory. Their finding showed that the critical temperature of sandwich plates is considerably increased by CNT reinforcement.

In the above discussed references, the CNTs' orientations were assumed to be straight and aligned, and the bulk mechanical properties of the composite are estimated by the rule of mixture. However, due to the low bending stiffness and high aspect ratio, CNTs tend to agglomerate in polymer matrices [25, 26]. Shi *et al.* [27] employed Eshelby's inclusion model to develop a micromechanics approach for assessing CNTs agglomeration effects. They demonstrated that CNT agglomeration significantly reduces the stiffness of the composite. Using the method in reference [27], Yas and Heshmati [28] studied the vibration of an FG-CNTRC beam traversed by a moving load, considering a random orientation of CNTs. Their result reveals that the random distribution of CNTs leads to higher beam deflections. The effects of CNT agglomeration and waviness on vibration of CNTRC beams were considered by Heshmati *et al.* [29, 30]. The DQM was employed by Mehrabadi and Aragh [31] to compute the stresses of agglomerated FG-CNTRC open cylindrical shells due to mechanical loading. Also using the DQM, Tornabene *et al.* [32] studied the distribution of stresses, strains, and displacements of composite plates and shells reinforced by agglomerated CNTs. The dynamic buckling of viscoelastic microplates reinforced by agglomerated CNTs is considered by Kolahchi and Cheraghba [33] using the Bolotin method in conjunction with the Navier method. Safaei *et al.* [34] investigated the thermal and mechanical buckling of porous sandwich plates formed from an isotropic core and CNTRC face layers. Galerkin method was used in references [35, 36] to investigate the vibration of agglomerated CNTRC plates and stability of nanocomposite beams, respectively. Kassa *et al.* [37] used the finite element method to study bending of CNTRC tapered panels, considering the CNT waviness and agglomeration effects. Based on the nonlocal elasticity theory, Daghigh *et al.* [38] derived the governing equations for bending and buckling analyses of CNTRC composite nanoplates. The two-parameter model in reference [27] was adopted to estimate the plate moduli and Navier's solution was employed to derive expressions for deflections and buckling loads.

In this paper, the large deflections of a CNTRC sandwich cantilever beam partially embedded on Pasternak foundation under end forces is studied considering the influence of CNTs agglomeration. The sandwich beam is composed of a homogeneous core and two composite face layers. The face layers are made from a polymer-based CNTs reinforced composite with effective elastic moduli being predicted by the Eshelby–Mori–Tanaka model. The discretized equilibrium is derived using a total Lagrangian nonlinear beam element, and solved by Newton–Raphson iterative method in combination with the arc-length technique. The effects of the CNT reinforcement, the agglomeration degree, the foundation support, and the porosities on the large deflection behavior of the sandwich cantilever beam are studied in detail.

2. Problem statement

Figure 1 shows a CNTRC sandwich cantilever with a rectangular cross-section ($b \times h$), partially embedded on a Pasternak foundation. The beam is formed from a homogeneous core and two CNTRC layers. The figure, x -axis is in the mid-plane; L and L_F are the lengths of the beam and foundation supporting part; z_0 , z_3 , z_1 , z_2 are coordinates in the z -direction of the bottommost and topmost surfaces, interfaces between the layers, respectively.

CNTs with high elastic moduli are used to reinforce polymer to enhance the stiffness of composite layers. The polymer core is fully characterized by elastic moduli of the polymer matrix, a homogenization scheme, namely the Eshelby–Mori–Tanaka model [39, 40], is used herein to predict elastic moduli of the composite faces. As mentioned above, CNTs tend to agglomerate in the polymer, creating a sort of spherical shaped inclusions, as depicted in Figure 2 for a representative volume element (RVE). CNTs in the RVE are found both in bundle or clusters inside the inclusions and scattered in the matrix. This particular distribution has been described by Shi *et al.* [27] by a two-parameter model, which is briefly summarized below.

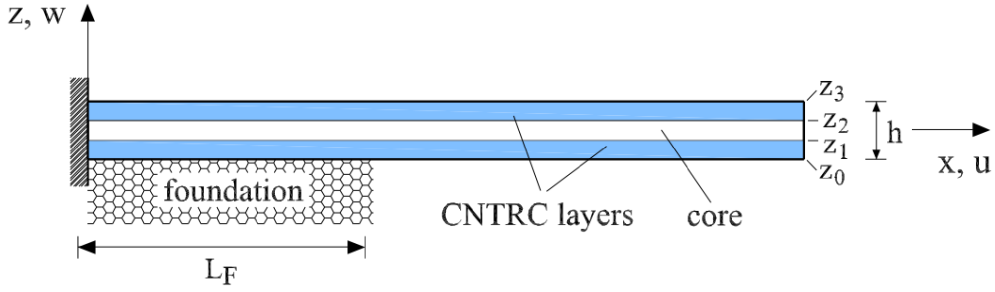


Figure 1. CNTRC sandwich cantilever beam partially embedded in Pasternak foundation.

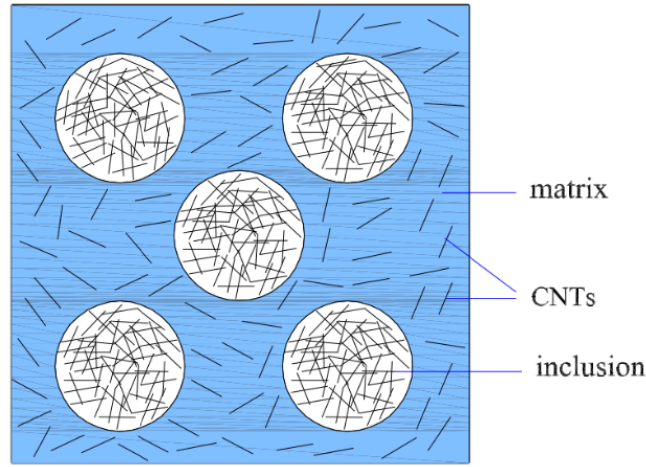


Figure 2. RVE with agglomerated CNT inclusions.

The total CNTs inside the RVE, (V_{CNT}), is split into two parts as follows

$$V_{\text{CNT}} = V_{\text{CNT}}^{\text{in}} + V_{\text{CNT}}^{\text{out}} \quad (1)$$

with $V_{\text{CNT}}^{\text{in}}$ and $V_{\text{CNT}}^{\text{out}}$ are, respectively, the volumes of CNTs inside and outside the inclusions.

The following parameters represent the CNT agglomeration

$$\xi = \frac{V_{\text{in}}}{V}, \quad \zeta = \frac{V_{\text{CNT}}^{\text{in}}}{V_{\text{CNT}}} \quad \text{with } (\xi, \zeta) \in [0, 1] \quad (2)$$

In Equation (2), the parameter ξ defines the volume proportion of inclusions (V_{in}) to the element volume (V), while parameter ζ quantifies the volume of CNTs inside inclusions ($V_{\text{CNT}}^{\text{in}}$) in respect of the total CNT volume. For $\xi < 1$, the agglomeration is partial with nanofillers are both in the inclusions and polymer matrix. The case $\xi = 1$ means that all CNTs are uniformly dispersed in the polymer, while $\zeta = 1$ corresponds to the case that all nanotubes are in the clusters.

The effective bulk and shear moduli inside the inclusions, (K_{in}) and (G_{in}), respectively, and that outside inclusions, (K_{out}) and (G_{out}), can be calculated as follows [27]

$$K_{\text{in}} = K_m + \frac{f_{\text{CNT}}\zeta(\delta_r - 3K_m\alpha_r)}{3(\xi - f_{\text{CNT}}\zeta + f_{\text{CNT}}\zeta\alpha_r)}, \quad G_{\text{in}} = G_m + \frac{f_{\text{CNT}}\zeta(\eta_r - 2G_m\beta_r)}{2(\xi - f_{\text{CNT}}\zeta + f_{\text{CNT}}\zeta\beta_r)} \quad (3)$$

and

$$\begin{aligned} K_{\text{out}} &= K_m + \frac{f_{\text{CNT}}(1-\zeta)(\delta_r - 3K_m\alpha_r)}{3[1-\xi - f_{\text{CNT}}(1-\zeta) + f_{\text{CNT}}(1-\zeta)\alpha_r]}, \\ G_{\text{out}} &= G_m + \frac{f_{\text{CNT}}(1-\zeta)(\eta_r - 2G_m\beta_r)}{2[1-\xi - f_{\text{CNT}}(1-\zeta) + f_{\text{CNT}}(1-\zeta)\beta_r]} \end{aligned} \quad (4)$$

with $f_{\text{CNT}} = V_{\text{CNT}}/V$, and

$$\begin{aligned} \alpha_r &= \frac{3(K_m + G_m) + k_r - l_r}{3(G_m + k_r)}, \quad \delta_r = \frac{1}{3} \left[n_r + 2l_r \frac{(2k_r + l_r)(3K_m + 2G_m - l_r)}{G_m + k_r} \right] \\ \beta_r &= \frac{1}{5} \left\{ \frac{4G_m + 2k_r + l_r}{3(G_m + k_r)} + \frac{4G_m}{G_m + p_r} + \frac{2G_m[(3K_m + G_m) + (3K_m + 7G_m)]}{G_m(3K_m + G_m) + m_r(3K_m + 7G_m)} \right\} \\ \eta_r &= \frac{1}{5} \left[\frac{2}{3}(n_r - l_r) + \frac{8G_m p_r}{G_m + p_r} + \frac{8m_r G_m(3K_m + 4G_m)}{3K_m(m_r + G_m) + G_m(7m_r + G_m)} + \frac{2(k_r - l_r)(2G_m + l_r)}{3(G_m + k_r)} \right] \end{aligned} \quad (5)$$

In the above equation, the subscript “*m*” and “*r*” are used to indicate the matrix and the reinforcement; k_r , m_r , n_r , l_r , and p_r are Hill’s elastic moduli of CNT reinforcement phase. It is noted that Equation (3) is not mathematically valid for $\xi = \zeta = 0$, while Equation (4) is not valid for $\xi = \zeta = 1$.

The bulk modulus and shear modulus of the composite are obtained by Mori–Tanaka homogenization model as

$$K = K_{\text{out}} \left[1 + \frac{\xi \left(\frac{K_{\text{in}}}{K_{\text{out}}} - 1 \right)}{1 + \alpha(1-\xi) \left(\frac{K_{\text{in}}}{K_{\text{out}}} - 1 \right)} \right], \quad G = G_{\text{out}} \left[1 + \frac{\xi \left(\frac{G_{\text{in}}}{G_{\text{out}}} - 1 \right)}{1 + \beta(1-\xi) \left(\frac{G_{\text{in}}}{G_{\text{out}}} - 1 \right)} \right] \quad (6)$$

where α and β are defines as

$$\alpha = \frac{1 + \nu_{\text{out}}}{3(1 - \nu_{\text{out}})}, \quad \beta = \frac{2(4 - 5\nu_{\text{out}})}{15(1 - \nu_{\text{out}})} \quad (7)$$

with $\nu_{\text{out}} = (3K_{\text{out}} - 2G_{\text{out}})/2(3K_{\text{out}} + G_{\text{out}})$. The effective Young’s modulus (E) and Poisson’s ratio (ν) of the composite are calculated as

$$E = \frac{9KG}{3K + G}, \quad \nu = \frac{3K - 2G}{6K + 2G} \quad (8)$$

The effective moduli estimated by the above equations do not consider the influence of porosities. The porosities have a negative effect on the elastic properties of the composite. For instance, an effective property (\mathcal{P}_{POR}) of the CNTRC material considering the porosity effect is given by [34]

$$\mathcal{P}_{\text{POR}} = (1 - f_p)\mathcal{P}, \quad f_p = 1 - \left(\frac{2}{\pi} \sqrt{1 - e_0} - \frac{2}{\pi} + 1 \right)^2 \quad (9)$$

with f_p is the porosity parameter, e_0 is the porosity coefficient, and \mathcal{P} is the effective property of the composite without porosities.

3. Solution method

A total Lagrangian beam element, initially proposed by Pacoste and Eriksson [41] and employed by Almeida *et al.* [42] as well as Nguyen *et al.* [43] to model geometric nonlinearity of functionally graded beams, is extended herewith to the CNTRC sandwich beam to construct the discretized equilibrium equation and to compute the response of the sandwich beam.

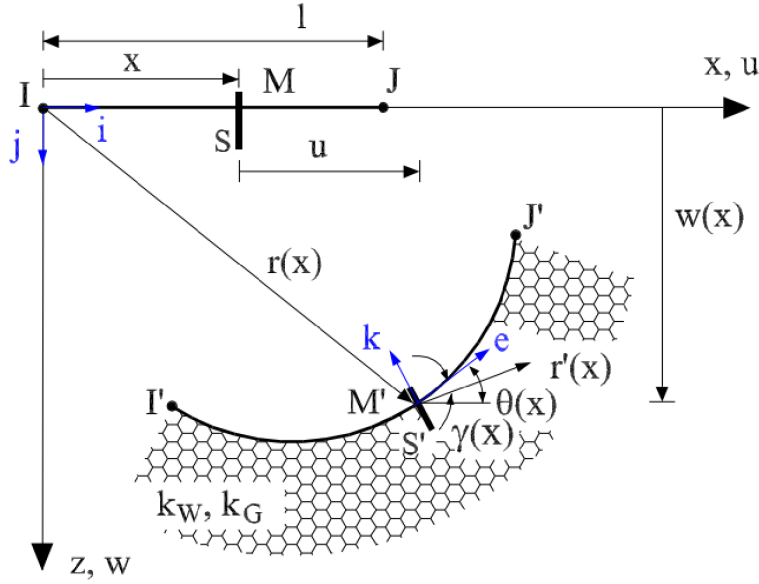


Figure 3. Initial and deformed configurations of the beam element on Pasternak foundation.

3.1. Total Lagrangian beam element

A two-node beam element, (I, J), initially straight as shown in Figure 3 is considered. The element is embedded on a Pasternak foundation with stiffness k_W and k_G of the Winkler and shear layers, respectively. The vector of nodal displacements and rotation has the form

$$\mathbf{d} = \{u_I \ w_I \ \theta_I \ u_J \ w_J \ \theta_J\}^T \quad (10)$$

in which u_I , w_I , θ_I respectively denote the displacements in the x and z directions and rotation at the node I, and the same for node J.

The current deformed configuration of the element, (I' , J'), is defined through the position vector \mathbf{r} of point M (see Figure 3), which is defined by

$$\mathbf{r} = [x + u(x)]\mathbf{i} + w(x)\mathbf{j} \quad (11)$$

In the above equation, \mathbf{i} and \mathbf{j} denote unit vectors of the x - and z -axes, while x is the abscissa of the point M, measured from the node I in the undeformed configuration; $u(x)$ and $w(x)$ are the displacements in x - and z -directions, respectively. The cross-section S associated with point M in the undeformed configuration undergoes large deflection and rotation to section S' related to point M' in the deformed configuration as depicted in Figure 3. The tangent vector \mathbf{r}' of the deformed line $I'J'$ at point M' is expressed in terms of the normal strain ε and the shear strain γ as

$$\mathbf{r}' = \frac{\partial \mathbf{r}}{\partial x} = [1 + \varepsilon]\mathbf{e} + \gamma\mathbf{k} \quad (12)$$

In the above equation, \mathbf{e} and \mathbf{k} are the unit vectors, orthogonal and parallel to the current section S' , and they are related to the base vectors \mathbf{i} and \mathbf{j} as

$$\mathbf{e} = \cos\theta\mathbf{i} + \sin\theta\mathbf{j}, \quad \mathbf{k} = -\sin\theta\mathbf{i} + \cos\theta\mathbf{j} \quad (13)$$

The curvature χ of the beam is defined as

$$\chi = \frac{\partial \theta}{\partial x} \quad (14)$$

From Equations (11)–(13), we can rewrite the normal and shear strains as follows

$$\varepsilon = \left(1 + \frac{\partial u}{\partial x}\right) \cos\theta + \frac{\partial w}{\partial x} \sin\theta - 1, \quad \gamma = \frac{\partial w}{\partial x} \cos\theta - \left(1 + \frac{\partial u}{\partial x}\right) \sin\theta \quad (15)$$

It should be emphasized that the strains ε , γ and the curvature χ although parameterized by the abscissa $x \in [0, 1]$, they take values on the current configuration.

The element strain energy U is contributed to the beam bending (U_B) and foundation deformation (U_F), $U = U_B + U_F$, in which

$$U_B = \frac{1}{2} \int_0^l (A_{11}\varepsilon^2 + 2A_{12}\varepsilon\chi + A_{22}\chi^2 + \psi A_{33}\gamma^2) dx \quad (16)$$

with $\psi = 5/6$ is the shear correction factor for the present beams and the rigidities A_{11} , A_{12} , A_{22} and A_{33} are defined as

$$(A_{11}, A_{12}, A_{22}) = \int_A (1, z, z^2) E dA = b \sum_{k=1}^3 \int_{z_{k-1}}^{z_k} (1, z, z^2) E dz, \quad A_{33} = \int_A G dA = b \sum_{k=1}^3 \int_{z_{k-1}}^{z_k} G dz \quad (17)$$

The effective moduli E and G in the above equation are dependent on the parameters ξ and ζ , as described in Section 2. One can notice that the coupling rigidity A_{12} in (17) will vanish when the two face layers are symmetric with respect to the mid-plane.

Since the beam undergoes large deflections, the foundation deformation in both the axial and transverse directions should be considered [44]. In this regard, the energy stored in the Pasternak foundation for the large deflection analysis is

$$U_F = \frac{k_W}{2} \int_0^{L_F} (u^2 + w^2) dx + \frac{k_G}{2} \int_0^{L_F} (\theta - \gamma)^2 dx \quad (18)$$

where, as above mentioned, k_W and k_G are the Winkler and shear moduli of the Pasternak foundation, and L_F is the foundation supporting length.

Interpolations are needed to be introduced for displacements and rotations. Since the displacements and rotation are independent from each another, the following linear interpolations can be employed

$$\begin{Bmatrix} u \\ w \\ \theta \end{Bmatrix} = \begin{bmatrix} \frac{l-x}{l} & 0 & 0 & \frac{x}{l} & 0 & 0 \\ 0 & \frac{l-x}{l} & 0 & 0 & \frac{x}{l} & 0 \\ 0 & 0 & \frac{l-x}{l} & 0 & 0 & \frac{x}{l} \end{bmatrix} \begin{Bmatrix} u_I \\ w_I \\ \theta_I \\ u_J \\ w_J \\ \theta_J \end{Bmatrix} \quad (19)$$

The element derived from the linear interpolations (19), however, suffers from the problem of shear locking. To avoid this locking problem, the reduced integration, namely one-point Gauss quadrature, is used in this work to calculate the terms associated with shear deformation in the strain energies in Equations (16) and (18). In this regard, the energy expression in Equations (16) and (18) can be written in the following forms

$$\begin{aligned} U_B &= \frac{l}{2} (A_{11}\hat{\varepsilon}^2 + 2A_{12}\hat{\varepsilon}\hat{\chi} + A_{22}\hat{\chi}^2 + \psi A_{33}\hat{\gamma}^2) \\ U_F &= \frac{lk_W}{6} (u_I^2 + u_I u_J + u_J^2 + w_I^2 + w_I w_J + w_J^2) + \frac{lk_G}{2} (\hat{\theta} - \hat{\gamma})^2 \end{aligned} \quad (20)$$

where

$$\begin{aligned}\hat{\varepsilon} &= \left(1 + \frac{u_J - u_I}{l}\right) \cos \hat{\theta} + \frac{w_J - w_I}{l} \sin \hat{\theta} - 1 \\ \hat{\gamma} &= -\left(1 + \frac{u_J - u_I}{l}\right) \sin \hat{\theta} + \frac{w_J - w_I}{l} \cos \hat{\theta} \\ \hat{\chi} &= \frac{\theta_J - \theta_I}{l} \quad \text{with } \hat{\theta} = \frac{\theta_I + \theta_J}{2}\end{aligned}\quad (21)$$

From Equation (21), one can compute

$$\begin{aligned}\frac{\partial \hat{\varepsilon}}{\partial u_I} &= -\frac{1}{l} \cos \hat{\theta}, & \frac{\partial \hat{\varepsilon}}{\partial u_J} &= \frac{1}{l} \cos \hat{\theta}, & \frac{\partial \hat{\varepsilon}}{\partial w_I} &= -\frac{1}{l} \sin \hat{\theta}, & \frac{\partial \hat{\varepsilon}}{\partial w_J} &= \frac{1}{l} \sin \hat{\theta} \\ \frac{\partial \hat{\gamma}}{\partial u_I} &= \frac{1}{l} \sin \hat{\theta}, & \frac{\partial \hat{\gamma}}{\partial u_J} &= -\frac{1}{l} \sin \hat{\theta}, & \frac{\partial \hat{\gamma}}{\partial w_I} &= -\frac{1}{l} \cos \hat{\theta}, & \frac{\partial \hat{\gamma}}{\partial w_J} &= \frac{1}{l} \cos \hat{\theta}, \\ \frac{\partial \hat{\varepsilon}}{\partial \theta_I} &= \frac{\partial \hat{\varepsilon}}{\partial \theta_J} = \frac{1}{2} \hat{\gamma}, & \frac{\partial \hat{\gamma}}{\partial \theta_I} &= \frac{\partial \hat{\gamma}}{\partial \theta_J} = -\frac{1}{2} (\hat{\varepsilon} + 1), & \frac{\partial \hat{\chi}}{\partial \theta_I} &= -\frac{\partial \hat{\chi}}{\partial \theta_J} = -\frac{1}{l}\end{aligned}\quad (22)$$

The element vector of nodal internal forces \mathbf{f}_{in} can be split into two parts, $\mathbf{f}_{\text{in}}^{\text{B}}$ due to beam bending and $\mathbf{f}_{\text{in}}^{\text{F}}$ due to foundation deformation, as follows

$$\mathbf{f}_{\text{in}} = \mathbf{f}_{\text{in}}^{\text{B}} + \mathbf{f}_{\text{in}}^{\text{F}} \quad (23)$$

These above internal force vectors are computed as derivatives of the strain energies in (19) respecting the element vector of nodal displacements as

$$\mathbf{f}_{\text{in}}^{\text{B}} = \frac{\partial U_{\text{B}}}{\partial \mathbf{d}} = \left\{ f_{u_I}^{\text{B}} \quad f_{w_I}^{\text{B}} \quad f_{\theta_I}^{\text{B}} \quad f_{u_J}^{\text{B}} \quad f_{w_J}^{\text{B}} \quad f_{\theta_J}^{\text{B}} \right\}^T, \quad \mathbf{f}_{\text{in}}^{\text{F}} = \frac{\partial U_{\text{F}}}{\partial \mathbf{d}} = \left\{ f_{u_I}^{\text{F}} \quad f_{w_I}^{\text{F}} \quad f_{\theta_I}^{\text{F}} \quad f_{u_J}^{\text{F}} \quad f_{w_J}^{\text{F}} \quad f_{\theta_J}^{\text{F}} \right\}^T \quad (24)$$

In substituting (20) into (24) and making use of Equation (22), one can obtain explicit expressions for the above element vectors of nodal forces. The detailed expressions for the coefficients of these vectors are given by Equations (A1) and (A2) in the Appendix.

The tangent stiffness matrix (\mathbf{k}_t) of the element can also be written in the form

$$\mathbf{k}_t = \mathbf{k}_t^{\text{B}} + \mathbf{k}_t^{\text{F}} \quad (25)$$

where \mathbf{k}_t^{B} and \mathbf{k}_t^{F} are the tangent stiffness matrices stemming from the deformation of the beam and the deformation, respectively. These matrices are computed by twice differentiation of the strain energy (20) with respect to the vector \mathbf{d} , and they have the forms

$$\mathbf{k}_t^{\text{B}} = \frac{\partial^2 U_{\text{B}}}{\partial \mathbf{d}^2} = \begin{bmatrix} k_{u_I u_I}^{\text{B}} & k_{u_I w_I}^{\text{B}} & k_{u_I \theta_I}^{\text{B}} & k_{u_I u_J}^{\text{B}} & k_{u_I w_J}^{\text{B}} & k_{u_I \theta_J}^{\text{B}} \\ & k_{w_I w_I}^{\text{B}} & k_{w_I \theta_I}^{\text{B}} & k_{w_I u_J}^{\text{B}} & k_{w_I w_J}^{\text{B}} & k_{w_I \theta_J}^{\text{B}} \\ & & k_{\theta_I \theta_I}^{\text{B}} & k_{\theta_I u_J}^{\text{B}} & k_{\theta_I w_J}^{\text{B}} & k_{\theta_I \theta_J}^{\text{B}} \\ & & & k_{u_J u_J}^{\text{B}} & k_{u_J w_J}^{\text{B}} & k_{u_J \theta_J}^{\text{B}} \\ \text{sym.} & & & & k_{w_J w_J}^{\text{B}} & k_{w_J \theta_J}^{\text{B}} \\ & & & & & k_{\theta_J \theta_J}^{\text{B}} \end{bmatrix} \quad (26)$$

and

$$\mathbf{k}_t^F = \frac{\partial^2 U_F}{\partial \mathbf{d}^2} = \begin{bmatrix} k_{u_1 u_1}^F & k_{u_1 w_1}^F & k_{u_1 \theta_1}^F & k_{u_1 u_j}^F & k_{u_1 w_j}^F & k_{u_1 \theta_j}^F \\ & k_{w_1 w_1}^F & k_{w_1 \theta_1}^F & k_{w_1 u_j}^F & k_{w_1 w_j}^F & k_{w_1 \theta_j}^F \\ & & k_{\theta_1 \theta_1}^F & k_{\theta_1 u_j}^F & k_{\theta_1 w_j}^F & k_{\theta_1 \theta_j}^F \\ & & & k_{u_j u_j}^F & k_{u_j w_j}^F & k_{u_j \theta_j}^F \\ \text{sym.} & & & & k_{w_j w_j}^F & k_{w_j \theta_j}^F \\ & & & & & k_{\theta_j \theta_j}^F \end{bmatrix} \quad (27)$$

The detailed expressions for the coefficients of the matrices \mathbf{k}_t^B and \mathbf{k}_t^F are listed by Equations (A3)–(A5) in the Appendix.

3.2. Equilibrium equation

After assembling the derived matrix \mathbf{k}_t and vector \mathbf{f}_{in} over the total number of elements, one can establish the nonlinear equilibrium equation for the beam in the following form [45]

$$\mathbf{g}(\mathbf{p}, \lambda) = \mathbf{q}_{in}(\mathbf{p}) - \lambda \mathbf{f}_{ef} \quad (28)$$

where \mathbf{g} is the residual force vector, is dependent on the vector of current nodal displacements \mathbf{p} and parameter of the load level λ ; \mathbf{q}_{in} is the global vector of nodal internal forces, obtained by merging vector \mathbf{f}_{in} over the total elements, and \mathbf{f}_{ef} is the vector of fixed external loads.

The nonlinear equations (28) is solved herein by Newton–Raphson iterative method, which contains predictor and corrector phases. In the method, a new solution is firstly predicted from the previously converged solution, and then corrected by iterative solutions. The following Euclidean norm based criterion is used for the iterative process

$$\|\mathbf{g}\| \leq \beta \|\lambda \mathbf{f}_{ef}\| \quad (29)$$

with β is a tolerance factor, chosen by 10^{-4} herein. The arc-length technique [45] is used with the above Newton–Raphson to trace the equilibrium paths when the beam exhibits complex nonlinear behavior.

4. Results and discussion

The sandwich cantilever beam is made from polymethyl methacrylate (PMMA) with $E^m = 2.5$ GPa, $\nu^m = 0.34$ as a matrix, and (10, 10) single-walled CNTs with the Hill's elastic moduli in Table 1 as reinforcement is considered. The beam is loaded by a transverse load P or a moment M at its free end. For the convenience of discussion, the non-dimensional parameters are employed

$$P^* = \frac{PL^2}{E^m I}, \quad M^* = \frac{ML}{E^m I}, \quad u^* = \frac{u_L}{L}, \quad w^* = \frac{w_L}{L}, \quad \theta^* = \frac{\theta}{2\pi} \quad (30)$$

where u_L and w_L are the axial and transverse displacements at the free end. Also, the dimensionless parameters for foundation stiffness supporting length are introduced as

$$k_1 = \frac{L^4 k_W}{E^m I}, \quad k_2 = \frac{L^2 k_G}{\pi^2 E^m I}, \quad \alpha_F = \frac{L_F}{L} \quad (31)$$

with k_W , k_G and L_F , as above mentioned, are the foundation stiffness and the length of the foundation supporting part. Except for Section 4.6, the results are reported for the perfect beams (without porosities).

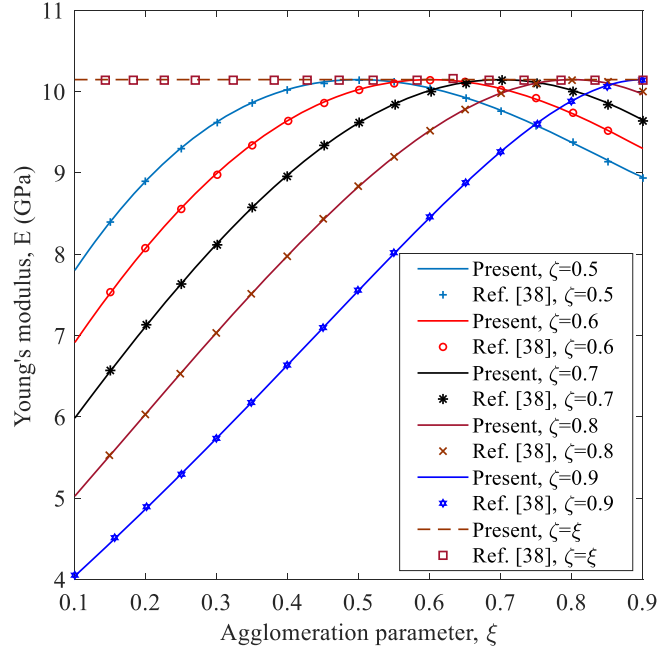


Figure 4. Comparison of effective Young's modulus of CNT reinforced composite with $V_{\text{CNT}} = 0.1$.

Table 1. Hill's elastic moduli for the carbon nanotubes [27]

Radius of CNTs (\AA)	k_r (GPa)	l_r (GPa)	m_r (GPa)	n_r (GPa)	p_r (GPa)
10	30	10	1	450	1

4.1. Verification

The derived formulation using the reduced integration has shown good performance in analyzing homogeneous beams with different aspect ratios in Ref. [41], the influence of the integration type on the solution is not presented herewith. The verification will focus on the accuracy and convergence of the formulation in modeling the large deflection of the CNT-reinforced composite beam. Firstly, the effective Young's modulus of the CNT-reinforced composite obtained in the present work is compared with the result of Daghighi et al. [38] in Figure 4 for a carbon nanotube volume fraction $V_{\text{CNT}} = 0.1$. One can see from the figure that the present result agrees well with that of the cited reference. It can also be seen from the figure that Young's modulus considerably decreases by the CNT agglomeration, and it attains the highest value when $\xi = \zeta$, which corresponds to the fully dispersed case.

In Table 2, the dimensionless tip displacements of a (1-2-1) CNTRC sandwich cantilever beam with $L/h = 20$ under an end moment $M^* = 5$ obtained herein are compared with the analytical solution of Refs. [46,47] for various values of the agglomerated parameters. The tip displacements of Refs. [46,47] are derived for an Euler–Bernoulli FG cantilever beam, and they have the following forms

$$u_L = L \left[1 - \frac{A_{22}}{ML} \sin \left(\frac{ML}{A_{22}} \right) \right], \quad w_L = \frac{A_{22}}{M} \left[1 - \cos \left(\frac{ML}{A_{22}} \right) \right] \quad (32)$$

where A_{22} is the bending stiffness, defined by Equation (17). An excellent agreement between the present result with the analytical solution of Refs. [46,47] is noted from Table 2, regardless of

Table 2. Comparison of tip displacements of symmetric (1-2-1) sandwich cantilever beam under end moment $M^* = 5$, $L/h = 20$ and $V_{\text{CNT}} = 0.1$

ζ		$\xi = 0.1$		$\xi = 0.3$		$\xi = 0.5$		$\xi = 0.7$	
		Present	Refs. [46, 47]	Present	Refs. [46, 47]	Present	Refs. [46, 47]	Present	Refs. [46, 47]
0.1	$ u^* $	0.2808	0.2810	0.3092	0.3093	0.3587	0.3589	0.4169	0.4171
	w^*	0.5815	0.5814	0.6025	0.6024	0.6342	0.6340	0.6644	0.6642
0.3	$ u^* $	0.3238	0.3239	0.2808	0.2810	0.3004	0.3006	0.3464	0.3466
	w^*	0.6124	0.6123	0.5815	0.5814	0.5963	0.5962	0.6268	0.6267
0.5	$ u^* $	0.4379	0.4381	0.3078	0.3079	0.2808	0.2810	0.3001	0.3002
	w^*	0.6737	0.6734	0.6015	0.6014	0.5815	0.5814	0.5960	0.5959
0.7	$ u^* $	0.6551	0.6553	0.4096	0.4098	0.3084	0.3085	0.2808	0.2810
	w^*	0.7241	0.7237	0.6610	0.6608	0.6019	0.6018	0.5815	0.5814
0.9	$ u^* $	1.0323	1.0323	0.6942	0.6943	0.4609	0.4610	0.3289	0.3291
	w^*	0.6150	0.6143	0.7250	0.7246	0.6828	0.6826	0.6158	0.6157

the agglomeration parameters. It is noted that, for the symmetric (1-2-1) sandwich beam under consideration, the coupling rigidity vanished, $A_{12} = 0$, and the analytical solution is derived by taking into account the neutral surface position, which allows to elimination of the coupling term.

The convergence of the derived beam element in predicting the large deflection response of the CNTRC beams is shown in Table 3, where the dimensionless deflections at the free end of symmetric (2-1-2) and nonsymmetric (1-1-2) sandwich cantilever beams with different aspect ratios under the tip load obtained by different number of elements (nELE) are given for $P^* = 10$, $V_{\text{CNT}} = 0.3$, $\alpha_F = 0.3$, $k_1 = 50$ and $k_2 = 0.2$. As seen from the table the convergence of both the symmetric (2-1-2) and non-symmetric (1-1-2) beams is achieved by using 24 elements, regardless of the agglomeration parameters and the aspect ratios. Because of this convergence result, a mesh of 24 elements is used in the computations reported below.

4.2. Effect of CNT reinforcement

In Table 4, the dimensionless tip displacements of (2-1-2) and (1-1-2) sandwich beams corresponding to $P^* = 10$ are given for $P^* = 10$, $L/h = 10$, $\alpha_F = 0.4$, $k_1 = 50$, and $k_2 = 0.5$. The influence of the CNT percentage and the agglomeration parameters on the beam response can be observed clearly from the table. As expected, the increase of V_{CNT} leads to a noticeable decrease in the tip displacements of both the symmetric and non-symmetric sandwich beams, regardless of the agglomeration parameters. The agglomeration degree of CNTs, indicated by the two parameters ξ and ζ , also has an impact on the beam response. The tip displacements of both the symmetric (2-1-2) and non-symmetric (2-2-1) beams attain the smallest values when $\xi = \zeta$, which corresponds to the fully dispersed case of CNTs. As mentioned above and shown in Figure 4, the effective Young's modulus of the composite attains the highest value when the CNTs are fully dispersed, and thus the beam stiffness is largest in this case. The tip response of both the sandwich beams is significant when the degree of CNT agglomeration is severe, which is the case of the two agglomerated parameters ξ and ζ are far from each other. A more detailed examination of the table shows that the effect of the CNT agglomeration is, however dependent on the CNT volume fraction, and this effect is more prominent for the beam associated with a higher CNT volume fraction. For example, the difference in the transverse displacements of the (2-1-2) beam associated with $V_{\text{CNT}} = 0.05$ for the cases of severe agglomeration ($\xi = 0.1$, $\zeta = 0.9$) and the full dispersion of

Table 3. Convergence of the formulation in predicting tip deflection w^* of the cantilever beam subjected to the tip load for $P^* = 10$, $V_{\text{CNT}} = 0.3$, $\alpha_F = 0.5$, $k_1 = 50$ and $k_2 = 0.2$

(ζ, ξ)	nELE	(2-1-2) beam				(1-1-2) beam			
		$L/h = 50$	$L/h = 20$	$L/h = 10$	$L/h = 5$	$L/h = 50$	$L/h = 20$	$L/h = 10$	$L/h = 5$
(0.1, 0.4)	8	0.5693	0.5703	0.5740	0.5889	0.7243	0.7276	0.7351	0.7565
	12	0.5697	0.5707	0.5744	0.5892	0.7245	0.7277	0.7352	0.7578
	16	0.5698	0.5708	0.5745	0.5894	0.7245	0.7278	0.7353	0.7581
	20	0.5698	0.5709	0.5746	0.5894	0.7245	0.7278	0.7353	0.7581
	22	0.5699	0.5709	0.5746	0.5895	0.7246	0.7278	0.7353	0.7581
	24	0.5699	0.5709	0.5746	0.5895	0.7246	0.7278	0.7353	0.7581
	26	0.5699	0.5709	0.5746	0.5895	0.7246	0.7278	0.7353	0.7581
(0.1, 0.6)	8	0.5945	0.5956	0.5965	0.6153	0.7397	0.7431	0.7508	0.7751
	12	0.5948	0.5959	0.5986	0.6156	0.7398	0.7432	0.7511	0.7753
	16	0.5955	0.5960	0.5998	0.6157	0.7415	0.7432	0.7512	0.7753
	20	0.5958	0.5961	0.6000	0.6158	0.7419	0.7433	0.7512	0.7753
	22	0.5978	0.5961	0.6001	0.6188	0.7424	0.7433	0.7512	0.7753
	24	0.5978	0.5961	0.6001	0.6158	0.7429	0.7433	0.7512	0.7753
	26	0.5978	0.5961	0.6001	0.6158	0.7429	0.7433	0.7512	0.7753

Table 4. Dimensionless tip displacements of CNTRC sandwich cantilever beam for $P^* = 10$, $L/h = 10$, $\alpha_F = 0.4$, $k_1 = 50$ and $k_2 = 0.5$

V_{CNT}	ζ		(2-1-2)				(1-1-2)			
			$\xi = 0.1$	$\xi = 0.3$	$\xi = 0.5$	$\xi = 0.7$	$\xi = 0.1$	$\xi = 0.3$	$\xi = 0.5$	$\xi = 0.7$
0.1	0.1	$ u^* $	0.5350	0.5421	0.5540	0.5679	0.6587	0.6636	0.6719	0.6815
		w^*	0.8088	0.8126	0.8190	0.8265	0.8774	0.8800	0.8843	0.8895
	0.3	$ u^* $	0.5463	0.5350	0.5402	0.5522	0.6665	0.6587	0.6623	0.6706
		w^*	0.8149	0.8088	0.8116	0.8181	0.8815	0.8774	0.8793	0.8837
	0.5	$ u^* $	0.5708	0.5418	0.5350	0.5402	0.6834	0.6634	0.6587	0.6623
		w^*	0.8280	0.8125	0.8088	0.8116	0.8905	0.8799	0.8774	0.8793
0.7	$ u^* $	0.6031	0.5625	0.5417	0.5350	0.7055	0.6777	0.6633	0.6587	
	w^*	0.8449	0.8236	0.8124	0.8088	0.9027	0.8874	0.8798	0.8774	
0.9	$ u^* $	0.6425	0.5987	0.5673	0.5452	0.7321	0.7025	0.6810	0.6658	
	w^*	0.8656	0.8427	0.8261	0.8143	0.9182	0.9010	0.8892	0.8811	
0.3	0.1	$ u^* $	0.1953	0.2132	0.2391	0.2577	0.3729	0.3925	0.4194	0.4377
		w^*	0.5406	0.5618	0.5902	0.6093	0.7139	0.7279	0.7459	0.7577
	0.3	$ u^* $	0.2214	0.1953	0.2073	0.2298	0.4013	0.3729	0.3862	0.4099
		w^*	0.5711	0.5406	0.5550	0.5803	0.7338	0.7139	0.7234	0.7397
	0.5	$ u^* $	0.2830	0.2129	0.1953	0.2066	0.4616	0.3922	0.3729	0.3854
		w^*	0.6336	0.5614	0.5406	0.5541	0.7723	0.7276	0.7139	0.7229
	0.7	$ u^* $	0.3823	0.2767	0.2142	0.1953	0.5460	0.4557	0.3936	0.3729
		w^*	0.7143	0.6277	0.5629	0.5406	0.8195	0.7688	0.7286	0.7139
	0.9	$ u^* $	0.5405	0.4348	0.3240	0.2324	0.6625	0.5864	0.4980	0.4126
		w^*	0.8118	0.7499	0.6694	0.5831	0.8794	0.8404	0.7934	0.7414

CNTs ($\xi = \zeta$) is 6.56%, while the corresponding value for the beam associated with $V_{\text{CNT}} = 0.3$ is 33.41%, which is more than five times higher.

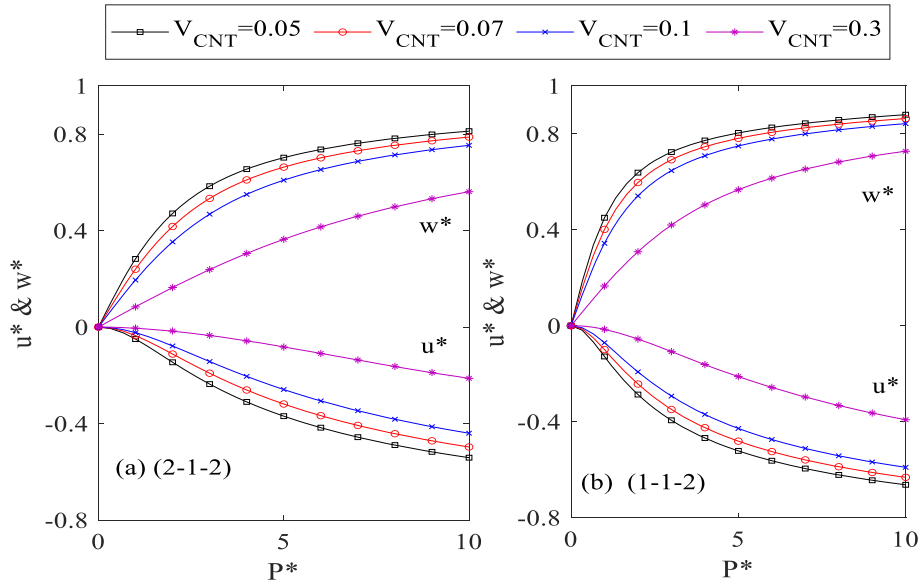


Figure 5. Effect of V_{CNT} on tip response of CNTRC sandwich beam under transverse load for $L/h = 10$, $\alpha_F = 0.4$, $(\xi, \zeta) = (0.4, 0.6)$ and $(k_1, k_2) = (50, 0.5)$.

To show the impact of CNT reinforcement on the beam response in more further, the effects of CNT volume fraction on the large deflection response of (2-1-2) symmetric and (1-1-2) non-symmetric sandwich cantilever beam under the tip load P and end moment M are respectively displayed in Figures 5 and 6 for $L/h = 10$, $\alpha_F = 0.4$, $(\xi, \zeta) = (0.4, 0.6)$ and $(k_1, k_2) = (50, 0.5)$. The effect of the degree of CNT agglomeration on the large deflections is shown in Figures 7 and 8, where the tip response of the symmetric (2-1-2) and non-symmetric (1-1-2) beams due to the tip transverse load and the end moment are depicted for $L/h = 10$, $V_{CNT} = 0.1$, $\alpha_F = 0.4$, $\zeta = 0.9$, $(k_1, k_2) = (50, 0.5)$ and different values of the agglomeration parameter ξ . Figure 5 shows a decline in the free end displacement of the sandwich cantilever beams by increasing the volume fraction of CNTs, regardless of the load level and the sandwich configuration. The influence of the CNT volume fraction on the response of the sandwich beam loaded by the end moment is seen in Figure 6, and the beam is more conservative in the case of a higher CNT volume fraction. The cantilever beam rolls up a half circle when the applied moment reaches a certain value, and after that the displacement w^* starts to decrease, as seen in Figure 6b for the curve corresponding to $V_{CNT} = 0.05$.

The tip response of the sandwich cantilever beam with the symmetric and non-symmetric configurations, as seen from 7 and 8, is more pronounced when the difference between the two agglomeration parameters ξ and ζ is larger. In other words, the more severe the agglomeration degree is, the larger tip displacements are, regardless of the loading type and the sandwich configuration. It is noted that the cantilever beam associated with $\xi = 0.3$ has rolled into a half circle when $M^* = 2$, and the displacement w^* decreases by increasing the moment some further, as seen in Figure 8b. Thus, though the displacement w^* of the beam with $\xi = 0.3$ loaded by $M^* > 2$ is smaller, it still deforms more significantly compared to the other cases ($\xi = 0.5, 0.7, 0.9$). The influence of the CNT reinforcement can also be observed from Figures 9 and 10, where the configurations in the deformed state of (2-1-2) and (1-1-2) beams due to the end moment are shown for $L/h = 10$, $\alpha_F = 0.4$, and $(k_1, k_2) = (50, 0.5)$. At the same applied moment parameter $M^* = 5$, the non-symmetric (1-1-2) beam with $V_{CNT} = 0.05$ has already rolled into

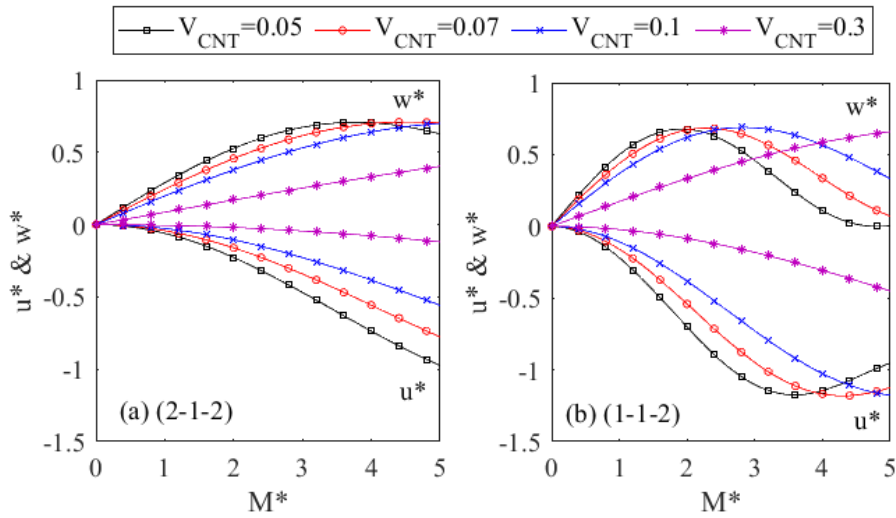


Figure 6. Effect of V_{CNT} on tip response of CNTRC sandwich beam under end moment for $L/h = 10$, $\alpha_F = 0.4$, $(\xi, \zeta) = (0.4, 0.6)$ and $(k_1, k_2) = (50, 0.5)$.

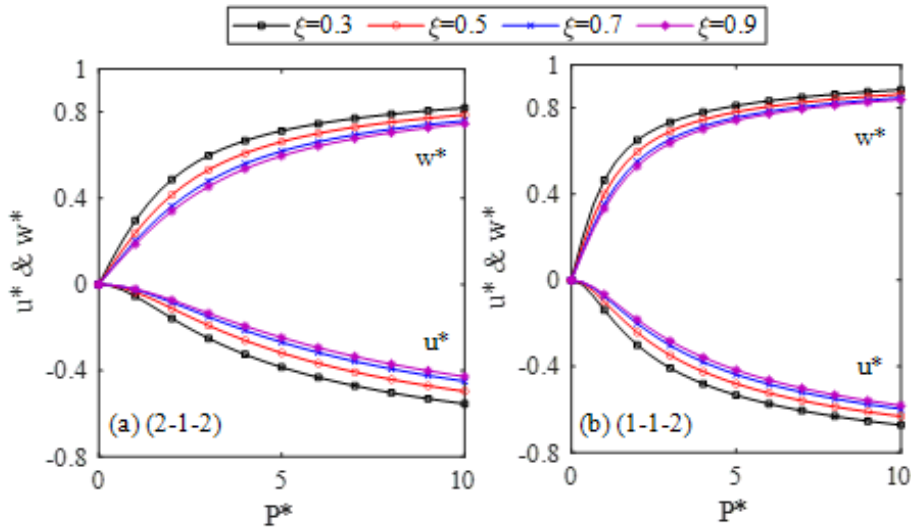


Figure 7. The tip response of CNTRC sandwich beam to transverse load for $L/h = 10$, $V_{CNT} = 0.1$, $\alpha_F = 0.4$, $\zeta = 0.9$, $(k_1, k_2) = (50, 0.5)$ and different values of ξ .

a circle, while the deformed curve of the (1-1-2) beam with $V_{CNT} = 0.3$ is still far from a haft circle (Figure 9b). The influence of the CNT volume fraction is seen more clearly from Table 5 where the dimensionless tip displacements and rotation of the sandwich beam with $L/h = 10$, $(\xi, \zeta) = (0.4, 0.7)$, $\alpha_F = 0.4$, $(k_1, k_2) = (50, 0.5)$ are given for $M^* = 3$ and $M^* = 5$. One can see that the beam associated with a lower V_{CNT} has larger tip rotation, regardless of the beam type and the applied moment. In other words, the beam with lower V_{CNT} deforms more significantly. The deformed configuration of the sandwich cantilever beams, as can be seen in Figure 10, is also significantly influenced by the agglomeration degree of CNTs. At $M^* = 5$, the non-symmetric

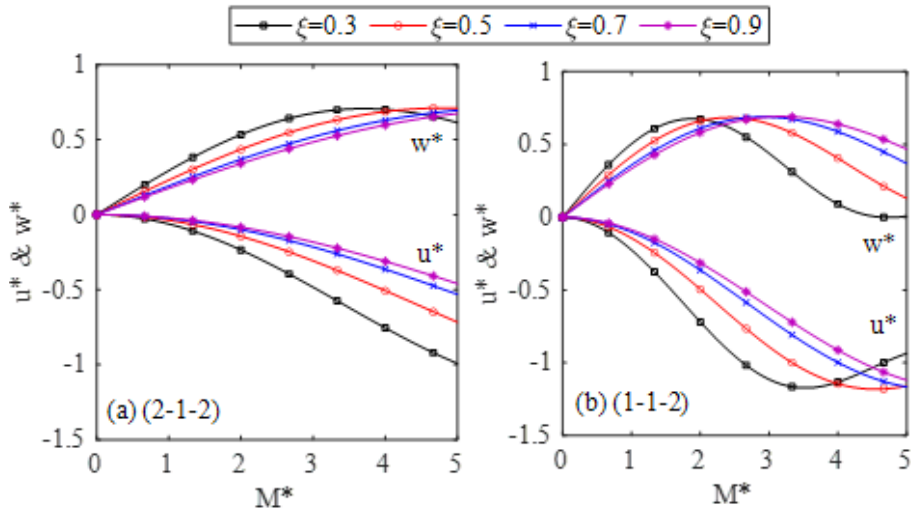


Figure 8. The tip response of CNTRC sandwich beam to the end moment for $L/h = 10$, $V_{CNT} = 0.1$, $\alpha_F = 0.4$, $\zeta = 0.9$, $(k_1, k_2) = (50, 0.5)$ and different values of ξ .

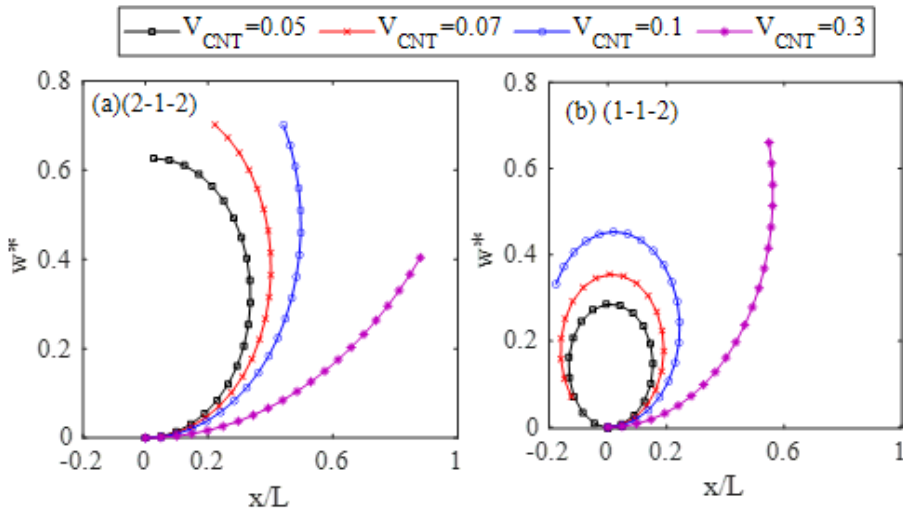


Figure 9. Deformed configurations of cantilever corresponding to $M^* = 5$ for $L/h = 10$, $(\xi, \zeta) = (0.4, 0.7)$, $\alpha_F = 0.4$, $(k_1, k_2) = (50, 0.5)$ and different values of V_{CNT} .

(1-1-2) sandwich beam with fully dispersed CNTs rolls into a haft circle, while the same beam with a severe degree of CNTs agglomeration ($\xi = 0.3$, $\zeta = 0.9$) has already rolled into a circle (Figure 10b).

4.3. Effect of foundation support

Figure 11 shows the load-deflection curves of the (2-1-2) symmetric and (1-1-2) non-symmetric sandwich cantilever beams under the tip load P for $L/h = 10$, $V_{CNT} = 0.1$, $(\xi, \zeta) = (0.4, 0.7)$, $\alpha_F = 0.4$ and different foundation stiffness parameters. The effect of the foundation supporting length is shown in Figure 12 for $L/h = 10$, $V_{CNT} = 0.1$, $(\xi, \zeta) = (0.4, 0.7)$, and $(k_1, k_2) = (50, 0.5)$. As expected,

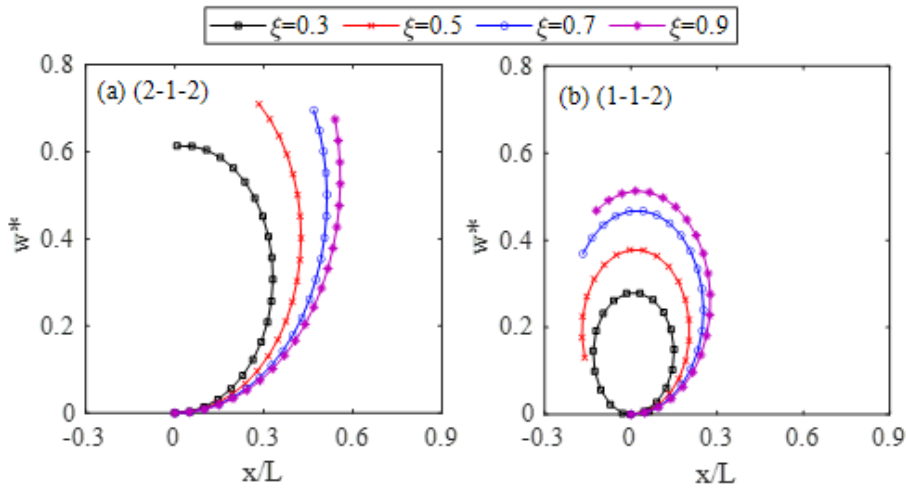


Figure 10. Deformed configurations of cantilever corresponding to $M^* = 5$ for $L/h = 10$, $\zeta = 0.9$, $\alpha_F = 0.4$, $(k_1, k_2) = (50, 0.5)$ and different values of ξ .

Table 5. Dimensionless tip displacements and rotation of CNTRC sandwich beam under end moment for $L/h = 10$, $(\xi, \zeta) = (0.4, 0.7)$, $\alpha_F = 0.4$, $(k_1, k_2) = (50, 0.5)$

M^*	Beam type	V_{CNT}				
		0.05	0.07	0.1	0.3	
3	(2-1-2)	$ u^* $	0.4689	0.3414	0.2279	0.0441
		w^*	0.6721	0.6144	0.5301	0.2523
		θ^*	0.2972	0.2461	0.1962	0.0830
	(1-1-2)	$ u^* $	1.1029	0.9481	0.7280	0.1821
		w^*	0.4587	0.6101	0.6863	0.4730
		θ^*	0.5997	0.4957	0.3959	0.1704
5	(2-1-2)	$ u^* $	0.9734	0.7774	0.5580	0.1198
		w^*	0.6262	0.7019	0.7010	0.4040
		θ^*	0.5008	0.4129	0.3282	0.1385
	(1-1-2)	$ u^* $	0.9525	1.1242	1.1766	0.4513
		w^*	0.0022	0.0708	0.3322	0.6603
		θ^*	1.0412	0.8550	0.6748	0.2848

the tip displacements are declined by increasing the foundation stiffness, irrespective of the load level and the sandwich configuration. The influence of the foundation supporting length on the large deflections of the sandwich beam is similar to that of the CNT volume fraction. One can see from Figures 11 and 12 that the increase of the supporting parameter α_F mitigates the tip displacements of the sandwich cantilever beam significantly, regardless of the loading type and the sandwich configuration.

4.4. Effect of sandwich configuration

The sandwich configuration, as can be seen from Table 4, has a significant impact on the large deflection response of the CNTRC sandwich cantilever beam. At the same volume fraction of

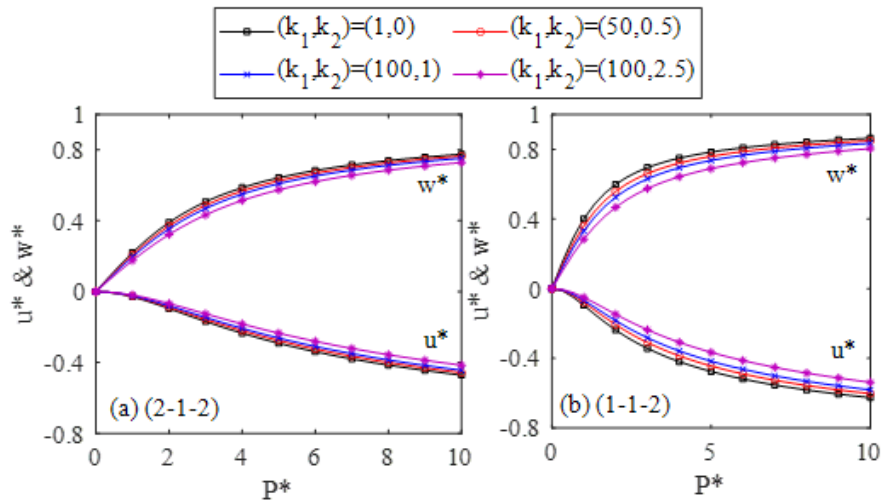


Figure 11. Effect of foundation stiffness on large deflections of CNTRC sandwich beams under transverse load for $L/h = 10$, $V_{CNT} = 0.1$, $(\xi, \zeta) = (0.4, 0.7)$, $\alpha_F = 0.4$.

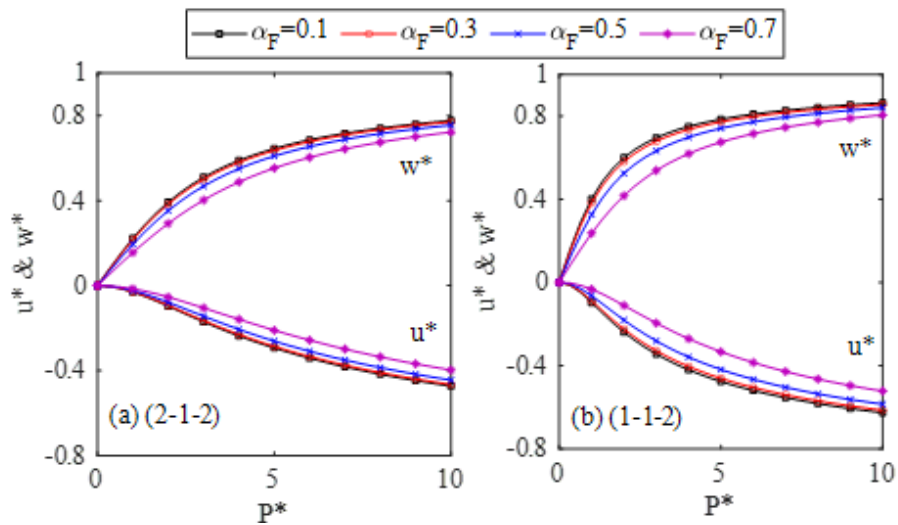


Figure 12. Effect of foundation supporting parameter on large deflections of sandwich beam under transverse load for $L/h = 10$, $V_{CNT} = 0.1$, $(\xi, \zeta) = (0.4, 0.7)$, $(k_1, k_2) = (50, 0.5)$.

the CNTs, the tip displacements of a non-symmetric (1-1-2) beam are considerably higher than that of the symmetric (2-1-2) beam, regardless of the CNT volume fraction and the agglomerated parameters. The deformed configurations of the sandwich beams under the end moment as depicted in Figures 9 and 10 also show the more conservative of the symmetric (2-1-2) beam compared to the non-symmetric (1-1-2) one. As seen from Figure 9, at the same end moment parameter $M^* = 5$, the non-symmetric (1-1-2) beam with $V_{CNT} = 0.05$ has rolled into a full circle, while the symmetric (2-1-2) beam just formed into a half circle only. The same situation is seen for the configurations of the (2-1-2) and (1-1-2) beams associated with $\xi = 0.05$ under the

Table 6. Tip displacements of CNTRC sandwich cantilever beams with different length-to-height ratios for $P^* = 10$, $V_{\text{CNT}} = 0.1$, $\alpha_F = 0.4$ and $(k_1, k_2) = (50, 0.5)$

L/h	ζ	(2-1-2)				(1-1-2)				
		$\xi = 0.1$	$\xi = 0.3$	$\xi = 0.5$	$\xi = 0.7$	$\xi = 0.1$	$\xi = 0.3$	$\xi = 0.5$	$\xi = 0.7$	
5	0.1	$ u^* $	0.4326	0.4459	0.4664	0.4871	0.5828	0.5927	0.6078	0.6229
		w^*	0.7707	0.7803	0.7947	0.8090	0.8749	0.8813	0.8913	0.9014
	0.3	$ u^* $	0.4522	0.4326	0.4419	0.4616	0.5974	0.5828	0.5897	0.6043
		w^*	0.7848	0.7707	0.7774	0.7913	0.8844	0.8749	0.8794	0.8889
	0.5	$ u^* $	0.4939	0.4452	0.4326	0.4418	0.6278	0.5922	0.5828	0.5896
		w^*	0.8137	0.7798	0.7707	0.7773	0.9047	0.8810	0.8749	0.8793
	0.7	$ u^* $	0.5505	0.4847	0.4455	0.4326	0.6675	0.6211	0.5924	0.5828
		w^*	0.8519	0.8074	0.7800	0.7707	0.9337	0.9002	0.8812	0.8749
10	0.1	$ u^* $	0.4280	0.4412	0.4617	0.4824	0.5813	0.5912	0.6063	0.6214
		w^*	0.7455	0.7540	0.7667	0.7791	0.8378	0.8429	0.8506	0.8582
	0.3	$ u^* $	0.4475	0.4280	0.4373	0.4569	0.5959	0.5813	0.5883	0.6028
		w^*	0.7579	0.7455	0.7515	0.7637	0.8453	0.8378	0.8414	0.8488
	0.5	$ u^* $	0.4892	0.4406	0.4280	0.4371	0.6263	0.5907	0.5813	0.5881
		w^*	0.7830	0.7536	0.7455	0.7513	0.8607	0.8426	0.8378	0.8413
	0.7	$ u^* $	0.5457	0.4800	0.4408	0.4280	0.6661	0.6196	0.5909	0.5813
		w^*	0.8146	0.7776	0.7537	0.7455	0.8813	0.8574	0.8427	0.8378
20	0.1	$ u^* $	0.4268	0.4400	0.4605	0.4812	0.5813	0.5912	0.6063	0.6214
		w^*	0.7391	0.7474	0.7596	0.7715	0.8265	0.8312	0.8384	0.8454
	0.3	$ u^* $	0.4464	0.4268	0.4361	0.4557	0.5959	0.5813	0.5882	0.6028
		w^*	0.7512	0.7391	0.7449	0.7568	0.8335	0.8265	0.8298	0.8367
	0.5	$ u^* $	0.4880	0.4394	0.4268	0.4359	0.6263	0.5907	0.5813	0.5881
		w^*	0.7753	0.7470	0.7391	0.7448	0.8477	0.8310	0.8265	0.8298
	0.7	$ u^* $	0.5445	0.4788	0.4397	0.4268	0.6661	0.6196	0.5909	0.5813
		w^*	0.8052	0.7702	0.7472	0.7391	0.8660	0.8446	0.8311	0.8265

end moment $M^* = 5$ in Figure 10. Thus, at given values of the CNT volume fraction and the agglomeration parameters, one can design a sandwich beam to mitigate the large deformation by the appropriate choice of the layer thickness ratio.

4.5. Effect of slenderness ratio

The length-to-height ratio, (L/h), of a rectangular cross-section beam represents the beam slenderness ratio. The dimensionless displacements at the free end of the (2-1-2) and (1-1-2) sandwich beams corresponding to a load parameter $P^* = 10$ are tabulated in Table 6 for $P^* = 10$, $V_{\text{CNT}} = 0.1$, $\alpha_F = 0.4$, $(k_1, k_2) = (50, 0.5)$ and different values of the length-to-height ratio and the agglomeration parameters. The table shows that the dimensionless tip displacements of both the sandwich cantilever beams are higher for the beams associated with a smaller length-to-height ratio, regardless of the agglomeration parameters and the sandwich configuration. One can also see from Table 6 that the effect of the slenderness ratio is dependent on the agglomeration parameters, which is on the agglomeration degree of CNTs. For example, for the fully dispersed case ($\xi = \zeta = 0.1$), the difference in the deflections of the symmetric (2-1-2) beam with $L/h = 5$ and $L/h = 20$ is 4.10% but this number increases to 5.48% for ($\xi = 0.1$, $\zeta = 0.7$), the case that

Table 7. Effect of porosities on the tip response of the sandwich cantilever beam under end moment for $L/h = 10$, $V_{\text{CNT}} = 0.07$, $\alpha_F = 0.4$, $(k_1, k_2) = (50, 0.5)$

Beam type	(ξ, ζ)	$M^* = 4$			$M^* = 8$			
		$f_p = 0$	$f_p = 0.1$	$f_p = 0.2$	$f_p = 0$	$f_p = 0.1$	$f_p = 0.2$	
(2-1-2)	(0.1, 0.1)	$ u^* $	0.4787	0.5638	0.6697	1.1445	1.1928	1.1939
		w^*	0.6787	0.6994	0.7082	0.4658	0.3426	0.1953
		θ^*	0.2992	0.3317	0.3723	0.6069	0.6754	0.7618
	(0.4, 0.7)	$ u^* $	0.5570	0.6506	0.7641	1.1905	1.1982	1.1470
		w^*	0.6982	0.7079	0.7001	0.3526	0.2205	0.0874
		θ^*	0.3291	0.3649	0.4097	0.6699	0.7459	0.8419
(1-1-2)	(0.1, 0.1)	$ u^* $	1.1260	1.1707	1.1714	0.8757	0.9295	1.0305
		w^*	0.4437	0.3256	0.1848	0.1247	0.1896	0.1815
		θ^*	0.6102	0.6782	0.7644	1.2610	1.3954	1.5612
	(0.4, 0.7)	$ u^* $	1.1685	1.1755	1.1273	0.9233	1.0137	1.0785
		w^*	0.3351	0.2089	0.0818	0.1864	0.1905	0.1050
		θ^*	0.6727	0.7486	0.8447	1.3847	1.5310	1.7135

the agglomeration degree of CNTs is the most severe. Since the length-to-height ratio indicates the shear deformation effect, one can say that the influence of the shear deformation is more remarkable when the agglomeration degree of CNTs is more severe. Examining Table 5 in more detail one can see that the effect of the slenderness ratio of the non-symmetric (1-1-2) sandwich beam is more significant than that of the symmetric (2-1-2) sandwich beam, regardless of the agglomeration degree. The difference between the deflections of non-symmetric (1-1-2) beams with $L/h = 5$ and $L/h = 20$ is 5.53% for the case of fully dispersed CNTs ($\xi = \zeta = 0.1$), and that is 7.25% for the case of severe degree of CNTs agglomeration ($\xi = 0.1$, $\zeta = 0.7$). These values are slightly higher than that of the symmetric (2-1-2) beam as stated above. The result in Table 5 reveals the ability of the derived formulation to model the influence of shear deformation on the large deflection response of the CNTRC sandwich beams.

4.6. Effect of porosities

The influence of porosities on large deflections of the CNTRC sandwich beam is examined in this Sub-section. Following the work in Ref. [34], the response of the beam is predicted for various values of the porosity parameter f_p . In Table 7, the dimensionless tip displacements and rotation of the porous beam with various porosity parameters are given for $L/h = 10$, $V_{\text{CNT}} = 0.07$, $\alpha_F = 0.4$, $(k_1, k_2) = (50, 0.5)$, and two values of the end moment, $M^* = 4$ and $M^* = 8$. The impact of the porosities on the large deflections is seen from the table, and the higher the porosity parameter is, the larger the tip rotation the beam has. The effect of the porosities on the large deformation of the CNTRC sandwich beam can also be seen in Figure 13, where the tip response and the deformed configurations of the (2-1-2) sandwich beam under a tip moment $M^* = 8$ are depicted for $L/h = 10$, $V_{\text{CNT}} = 0.07$, $\xi = 0.4$, $\zeta = 0.7$, $\alpha_F = 0.4$, $(k_1, k_2) = (50, 0.5)$ and different values of the porosity parameter. Figure 13b shows that the beam associated with a higher porosity parameter deforms more significantly, though the deflection corresponding to $M^* = 8$ in Figure 13a decreases by increasing f_p . The increase of the tip rotation by increasing the porosity parameter as seen in Table 7 also confirms the influence of the porosities on the large deflections of the beam.

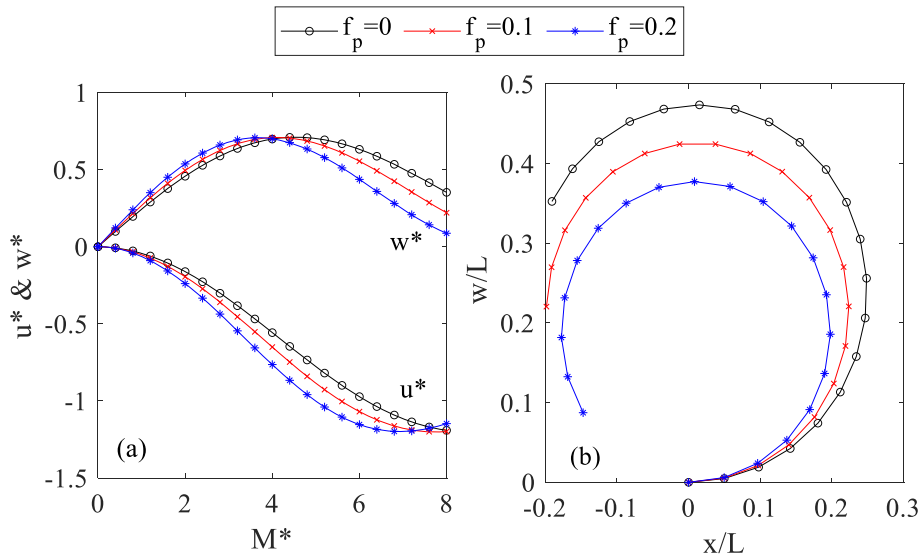


Figure 13. The tip response and deformed configurations of CNTRC (2-1-2) beam according to $M^* = 8$ for $L/h = 10$, $V_{\text{CNT}} = 0.07$, $\xi = 0.4$, $\zeta = 0.7$, $\alpha_F = 0.4$, $(k_1, k_2) = (50, 0.5)$ and different values of f_p .

5. Conclusions

The large deflections of the CNTRC sandwich cantilever beam partially embedded on a Pasternak foundation under the end forces have been studied considering the influence of CNTs agglomeration. The sandwich beam is composed of homogeneous and two face layers made from a CNT-reinforced composite. Eshelby–Mori–Tanaka model has been applied to predict the effective moduli of the composite. Based on the first-order shear deformation theory, a total Lagrangian beam element was derived and used to establish the equilibrium equation for the beam. The Newton–Raphson method was used in conjunction with the arc-length technique to compute the load-displacement curves. The effects of various important factors, including the CNT volume fraction, CNT agglomeration parameters, porosities, foundation stiffness and supporting length on the large deflection response of the beam have been studied in detail. The finding shows that the sandwich cantilever beam is more conservative for a higher CNT volume fraction and a longer supporting part. The agglomeration of CNTs has an important role in the behavior of the sandwich beam, and it not only makes the beam more flexible but also raises the effect of the shear deformation on the large deflections. It was also shown that the sandwich configuration is important in the behavior of the CNTRC sandwich beam and the symmetric beam tends to be more conservative than the non-symmetric one.

Declaration of interests

The authors do not work for, advise, own shares in, or receive funds from any organization that could benefit from this article, and have declared no affiliations other than their research organizations.

Data availability statement

The paper is self-contained and uses no external data.

Funding

This research is funded by Vietnam National Foundation for Science and Technology Development (NAFOSTED) under grant number 107.02-2021.11.

Appendix A.

This Appendix lists the coefficients of the internal force vectors and tangent stiffness matrices in Equations (24), (26) and (27).

(1) Components of the internal force vectors in Equation (24)

$$\begin{aligned}
 f_{u_I}^B &= -(A_{11}\hat{\varepsilon} + A_{12}\hat{\chi}) \cos \hat{\theta} + \psi A_{33}\hat{\gamma} \sin \hat{\theta}, & f_{w_I}^B &= -(A_{11}\hat{\varepsilon} + A_{12}\hat{\chi}) \sin \hat{\theta} - \psi A_{33}\hat{\gamma} \cos \hat{\theta} \\
 f_{\theta_I}^B &= \frac{l}{2} A_{11}\hat{\varepsilon}\hat{\gamma} + \frac{l}{2} A_{12} \left(\hat{\gamma}\hat{\chi} - \frac{2}{l}\hat{\varepsilon} \right) - A_{22}\hat{\chi} - \frac{l}{2} \psi A_{33} (\hat{\varepsilon} + 1) \hat{\gamma} \\
 f_{u_J}^B &= (A_{11}\hat{\varepsilon} + A_{12}\hat{\chi}) \cos \hat{\theta} - \psi A_{33}\hat{\gamma} \sin \hat{\theta}, & f_{w_J}^B &= (A_{11}\hat{\varepsilon} + A_{12}\hat{\chi}) \sin \hat{\theta} + \psi A_{33}\hat{\gamma} \cos \hat{\theta} \\
 f_{\theta_J}^B &= \frac{l}{2} A_{11}\hat{\varepsilon}\hat{\gamma} + A_{12} \left(\frac{l}{2}\hat{\gamma}^2 - \hat{\varepsilon} \right) + A_{22}\hat{\chi} - \frac{l}{2} \psi A_{33} (\hat{\varepsilon} + 1) \hat{\gamma}
 \end{aligned} \tag{A1}$$

and

$$\begin{aligned}
 f_{u_I}^F &= \frac{l}{6} k_W (2u_I + u_J) + k_G (\hat{\theta} - \hat{\gamma}) \sin \hat{\theta}, & f_{w_I}^F &= \frac{l}{6} k_W (2w_I + w_J) + k_G (\hat{\theta} - \hat{\gamma}) \cos \hat{\theta} \\
 f_{\theta_I}^F &= l k_G (\hat{\theta} - \hat{\gamma}) \left(1 - \frac{l}{2} \hat{\varepsilon} \right), & f_{u_J}^F &= \frac{l}{6} k_W (u_I + 2u_J) + k_G (\hat{\theta} - \hat{\gamma}) \sin \hat{\theta} \\
 f_{w_J}^F &= \frac{l}{6} k_W (w_I + 2w_J) - k_G (\hat{\theta} - \hat{\gamma}) \cos \hat{\theta}, & \text{and } f_{\theta_J}^F &= f_{\theta_I}^F
 \end{aligned} \tag{A2}$$

(2) Coefficients of the tangent stiffness matrices in Equations (26) and (27)

- The diagonal coefficients of the matrix \mathbf{k}_t^B in (26)

$$\begin{aligned}
 k_{u_I u_I}^B &= \frac{1}{l} (A_{11} \cos^2 \hat{\theta} + \psi A_{33} \sin^2 \hat{\theta}), & k_{w_I w_I}^B &= \frac{1}{l} (A_{11} \sin^2 \hat{\theta} + \psi A_{33} \cos^2 \hat{\theta}) \\
 k_{\theta_I \theta_I}^B &= \frac{l A_{11}}{4} [\hat{\gamma}^2 - \hat{\varepsilon} (\hat{\varepsilon} + 1)] - \frac{l A_{12}}{4} \left[(\hat{\varepsilon} + 1) \hat{\chi} + \frac{4}{l} \hat{\gamma} \right] + \frac{A_{22}}{l} + \frac{l \psi A_{33}}{4} [(\hat{\varepsilon} + 1)^2 - \hat{\gamma}^2] \\
 k_{\theta_I \theta_J}^B &= \frac{l A_{11}}{4} [\hat{\gamma}^2 - \hat{\varepsilon} (\hat{\varepsilon} + 1)] - \frac{l A_{12}}{4} (\hat{\varepsilon} + 1) \hat{\chi} + \frac{A_{22}}{l} + \frac{l \psi A_{33}}{4} [(\hat{\varepsilon} + 1)^2 - \hat{\gamma}^2] \\
 \text{and } k_{u_I u_J}^B &= k_{u_I u_I}^B, & k_{w_I w_J}^B &= k_{w_I w_I}^B.
 \end{aligned} \tag{A3}$$

- The non-diagonal coefficients of the stiffness matrix \mathbf{k}_t^B in (26)

$$\begin{aligned}
 k_{u_I w_I}^B &= \frac{A_{11}}{l} \sin \hat{\theta} \cos \hat{\theta} - \frac{\psi A_{33}}{l} \sin \hat{\theta} \cos \hat{\theta} \\
 k_{u_I \theta_I}^B &= \frac{A_{11}}{2} (\hat{\varepsilon} \sin \hat{\theta} - \hat{\gamma} \cos \hat{\theta}) - \frac{A_{12}}{2l} (\hat{\chi} \sin \hat{\theta} + 2 \cos \hat{\theta}) + \frac{\psi A_{33}}{2} [\hat{\gamma} \cos \hat{\theta} - (\hat{\varepsilon} + 1) \sin \hat{\theta}] \\
 k_{w_I \theta_I}^B &= -\frac{A_{11}}{2} (\hat{\gamma} \sin \hat{\theta} + \hat{\varepsilon} \cos \hat{\theta}) + \frac{A_{12}}{2l} (l \hat{\chi} \cos \hat{\theta} - 2 \sin \hat{\theta}) + \frac{\psi A_{33}}{2} [\hat{\gamma} \sin \hat{\theta} + (\hat{\varepsilon} + 1) \cos \hat{\theta}] \\
 k_{w_I \theta_J}^B &= -\frac{A_{11}}{2} (\hat{\gamma} \sin \hat{\theta} + \hat{\varepsilon} \cos \hat{\theta}) + \frac{A_{12}}{2l} (l \hat{\chi} \cos \hat{\theta} + 2 \sin \hat{\theta}) + \frac{\psi A_{33}}{2} [\hat{\gamma} \sin \hat{\theta} + (\hat{\varepsilon} + 1) \cos \hat{\theta}] \\
 k_{u_I \theta_J}^B &= \frac{A_{11}}{2} (\hat{\varepsilon} \sin \hat{\theta} - \hat{\gamma} \cos \hat{\theta}) + \frac{A_{12}}{2l} (\hat{\chi} \sin \hat{\theta} - 2 \cos \hat{\theta}) + \frac{\psi A_{33}}{2} [\hat{\gamma} \cos \hat{\theta} - (\hat{\varepsilon} + 1) \sin \hat{\theta}]
 \end{aligned} \tag{A4}$$

and

$$\begin{aligned}
 k_{u_I u_J}^B &= -k_{u_I u_I}^B, & k_{u_I w_J}^B &= -k_{u_I w_I}^B, & k_{u_I \theta_I}^B &= k_{u_I \theta_I}^B, & k_{w_I w_J}^B &= -k_{w_I w_I}^B, \\
 k_{w_I \theta_I}^B &= -k_{w_I \theta_I}^B, & k_{u_J w_I}^B &= k_{u_I w_I}^B, & k_{u_J \theta_I}^B &= -k_{u_I \theta_I}^B, & k_{w_J \theta_I}^B &= -k_{w_I \theta_I}^B
 \end{aligned}$$

- The coefficients of the stiffness matrix \mathbf{k}_t^F in (27)

$$k_{u_1 u_1}^F = \frac{l}{3} k_W + \frac{1}{l} \sin^2 \hat{\theta} k_G, \quad k_{w_1 w_1}^F = \frac{l}{3} k_W + \frac{1}{l} \cos^2 \hat{\theta} k_G, \quad k_{\theta_1 \theta_1}^F = \frac{l}{4} [(2 - \hat{\varepsilon})^2 - (\hat{\theta} - \hat{\gamma}) \hat{\gamma}] k_G, \\ k_{u_1 w_1}^F = -\frac{1}{2l} \sin 2\hat{\theta} k_G \quad (A5)$$

$$k_{u_1 \theta_1}^F = -\frac{1}{2} [(2 - \hat{\varepsilon}) \sin \hat{\theta} - (\hat{\theta} - \hat{\gamma}) \cos \hat{\theta}] k_G, \quad k_{w_1 \theta_1}^F = \frac{1}{2} [(2 - \hat{\varepsilon}) \cos \hat{\theta} - (\hat{\theta} - \hat{\gamma}) \sin \hat{\theta}] k_G$$

and

$$k_{u_1 u_j}^F = k_{u_j u_1}^F, \quad k_{u_1 u_j}^F = -k_{u_j u_1}^F, \quad k_{w_1 w_j}^F = k_{w_j w_1}^F, \quad k_{w_1 w_j}^F = -k_{w_j w_1}^F, \quad k_{\theta_1 \theta_j}^F = k_{\theta_j \theta_1}^F = k_{\theta_1 \theta_j}^F, \\ k_{u_1 w_j}^F = k_{u_j w_1}^F, \quad k_{u_1 w_j}^F = -k_{u_j w_1}^F, \quad k_{u_1 \theta_j}^F = k_{\theta_j u_1}^F, \quad k_{w_1 \theta_j}^F = k_{\theta_j w_1}^F, \quad k_{w_1 \theta_j}^F = -k_{\theta_j w_1}^F$$

References

- [1] Y. Saito, K. Hamaguchi, K. Hata *et al.*, "Conical beams from open nanotubes", *Nature* **389** (1997), p. 554-555.
- [2] E. T. Thostenson, Z. Ren, T. W. Chou, "Advances in the science and technology of carbon nanotubes and their composites: a review", *Compos. Sci. Technol.* **61** (2010), p. 1899-1912.
- [3] J. D. Fidelus, E. Wiesel, F. H. Gojny *et al.*, "Thermomechanical properties of randomly oriented carbon/epoxy nanocomposites", *Composites A* **36** (2005), no. 11, p. 1555-1561.
- [4] J. N. Coleman, U. Khan, W. J. Blau *et al.*, "Small but strong: a review of the mechanical properties of carbon nanotube-polymer composites", *Carbon* **44** (2006), no. 9, p. 1624-1652.
- [5] K. M. Liew, Z. X. Lei, L. W. Zhang, "Mechanical analysis of functionally graded carbon nanotube reinforced composites: a review", *Compos. Struct.* **120** (2015), p. 90-97.
- [6] S. I. Yengejeh, S. A. Kazemi, A. Öchsner, "Carbon nanotubes as reinforcement in composites: A review of the analytical, numerical, and experimental approaches", *Comput. Mater. Sci.* **136** (2017), p. 85-101.
- [7] S. H. Shen, "Nonlinear bending of functionally graded carbon nanotube-reinforced composite plates in thermal environments", *Compos. Struct.* **91** (2009), p. 9-19.
- [8] S. H. Shen, Z. H. Zhu, "Postbuckling of sandwich plates with nanotube-reinforced composite face sheets resting on elastic foundations", *Eur. J. Mech. A Solids* **35** (2012), p. 10-21.
- [9] H. S. Shen, Y. Xiang, "Nonlinear analysis of nanotube-reinforced composite beams resting on elastic foundations in thermal environments", *Eng. Struct.* **56** (2013), p. 698-708.
- [10] N. Wattanasakulpong, V. Ungbhakorn, "Analytical solutions for bending, buckling and vibration responses of carbon nanotube-reinforced composite beams resting on elastic foundation", *Comput. Mater. Sci.* **71** (2013), p. 201-208.
- [11] K. Mayandi, P. Jeyaraj, "Bending, buckling and free vibration characteristics of FG-CNT-reinforced polymer composite beam under non-uniform thermal load", *Proc. Inst. Mech. Eng. L* **229** (2015), p. 13-28.
- [12] Z. X. Lei, K. M. Liew, J. L. Yu, "Large deflection analysis of functionally graded carbon nanotube-reinforced composite plates by the element-free kp -Ritz method", *Comput. Methods Appl. Mech. Eng.* **256** (2013), p. 189-199.
- [13] L. W. Zhang, Z. X. Lei, K. M. Liew *et al.*, "Large deflection geometrically nonlinear analysis of carbon nanotube-reinforced functionally graded cylindrical panels", *Comput. Methods Appl. Mech. Eng.* **273** (2014), p. 1-18.
- [14] K. M. Liew, Z. X. Lei, J. L. Yu *et al.*, "Postbuckling of carbon nanotube-reinforced functionally graded cylindrical panels under axial compression using a meshless approach", *Comput. Methods Appl. Mech. Eng.* **268** (2014), p. 1-17.
- [15] L. W. Zhang, K. M. Liew, J. N. Reddy, "Postbuckling of carbon nanotube reinforced functionally graded plates with edges elastically restrained against translation and rotation under axial compression", *Comput. Methods Appl. Mech. Eng.* **298** (2016), p. 1-28.
- [16] L. W. Zhang, K. M. Liew, Z. Jiang, "An element-free analysis of CNT-reinforced composite plates with column supports and elastically restrained edges under large deformation", *Composites B* **95** (2016), p. 18-28.
- [17] L. W. Zhang, "Geometrically nonlinear large deformation of CNT-reinforced composite plates with internal column supports", *J. Model. Mech. Mater.* **1** (2017), article no. 20160154.
- [18] S. Zghal, A. Frikha, F. Dammak, "Large deflection response-based geometrical nonlinearity of nanocomposite structures reinforced with carbon nanotubes", *Appl. Math. Mech.* **41** (2020), p. 1227-1250.
- [19] S. Natarajan, M. Haboussi, G. Manickam, "Application of higher-order structural theory to bending and free vibration analysis of sandwich plates with CNT reinforced composite facesheets", *Compos. Struct.* **13** (2014), p. 197-207.
- [20] H. Wu, S. Kitipornchai, J. Yang, "Free vibration and buckling analysis of sandwich beams with functionally graded carbon nanotube-reinforced composite face sheets", *Int. J. Struct. Stab. Dynam.* **15** (2015), no. 7, p. 1540011-1540027.
- [21] A. Sankar, S. El-Borgicd, T. B. Zinebef *et al.*, "Dynamic snap-through buckling of CNT reinforced composite sandwich spherical caps", *Composites B* **99** (2016), p. 472-482.

- [22] A. Sankar, S. El-Borgicd, M. Ganapathia, "Parametric instability of thick doubly curved CNT reinforced composite sandwich panels under in-plane periodic loads using higher-order shear deformation theory", *J. Vib. Control.* **24** (2018), no. 10, p. 1927-1950.
- [23] K. Mehar, S. K. Panda, B. K. Patle, "Stress, deflection, and frequency analysis of CNT reinforced graded sandwich plate under uniform and linear thermal environment: A finite element approach", *Polym. Compos.* **39** (2018), no. 10, p. 3792-3809.
- [24] S. Kamarian, M. Bodaghi, R. B. Isfahani *et al.*, "Thermal buckling analysis of sandwich plates with soft core and CNT-Reinforced composite face sheets", *J. Sand. Struct. Mater.* **23** (2021), no. 8, p. 3606-3644.
- [25] M. S. P. Shaffer, A. H. Windle, "Fabrication and characterization of carbon nanotube/poly (vinyl alcohol) composites", *Adv. Mater.* **11** (1999), no. 11, p. 937-941.
- [26] B. Vigolo, A. Penicaud, C. Coulon *et al.*, "Macroscopic fibers and ribbons of oriented carbon nanotubes", *Science* **290** (2000), p. 1331-1334.
- [27] D. L. Shi, X. Q. Feng, Y. Y. Huang *et al.*, "The effect of nanotube waviness and agglomeration on the elastic property of carbon nanotube-reinforced composites", *J. Eng. Mater. Technol.* **126** (2004), no. 3, p. 250-257.
- [28] M. H. Yas, M. Heshmati, "Dynamic analysis of functionally graded nanocomposite beams reinforced by randomly oriented carbon nanotube under the action of moving load", *Appl. Math. Model.* **36** (2012), no. 4, p. 1371-1394.
- [29] M. Heshmati, M. H. Yas, "Free vibration analysis of functionally graded CNT reinforced nanocomposite beam using Eshelby-Mori-Tanaka approach", *J. Mech. Sci. Technol.* **27** (2013), p. 3403-3408.
- [30] M. Heshmati, M. H. Yas, F. Daneshmand, "A comprehensive study on the vibrational behavior of CNT-reinforced composite beams", *Compos. Struct.* **125** (2015), p. 434-448.
- [31] S. J. Mehrabadi, B. S. Aragh, "Stress analysis of functionally graded open cylindrical shell reinforced by agglomerated carbon nanotubes", *Thin-Walled Struct.* **80** (2014), p. 130-141.
- [32] F. Tornabene, N. Fantuzzi, M. Baccocchi, "Linear static response of nanocomposite plates and shells reinforced by agglomerated carbon nanotubes", *Composites B* **115** (2017), p. 449-476.
- [33] R. Kolahchi, A. Cheraghbak, "Agglomeration effects on the dynamic buckling of viscoelastic microplates reinforced with SWCNTs using Bolotin method", *Nonlinear Dyn.* **90** (2017), no. 1, p. 479-492.
- [34] B. Safaei, R. Moradi-Dastjerdi, K. Behdinan *et al.*, "Critical buckling temperature and force in porous sandwich plates with CNT-reinforced nanocomposite layers", *Aerosp. Sci. Technol.* **91** (2019), p. 75-185.
- [35] F. Ebrahimi, A. Dabbagh, A. Rastgoo, "Free vibration analysis of multi-scale hybrid nanocomposite plates with agglomerated nanoparticles", *Mech. Based Des. Struct.* **49** (2019), p. 487-510.
- [36] A. Dabbagh, A. Rastgoo, F. Ebrahimi, "Static stability analysis of agglomerated multi-scale hybrid nanocomposites via a refined theory", *Eng. Comput.* **37** (2021), p. 2225-2244.
- [37] M. K. Kassa, R. Selvaraj, H. D. Wube *et al.*, "Investigation of the bending response of carbon nanotubes reinforced laminated tapered spherical composite panels with the influence of waviness, interphase and agglomeration", *Mech. Based Des. Struct.* **51** (2021), p. 5902-5924.
- [38] H. Daghigh, V. Daghigh, A. Milani *et al.*, "Nonlocal bending and buckling of agglomerated CNT-reinforced composite nanoplates", *Composites B* **183** (2020), article no. 107716.
- [39] J. D. Eshelby, "The determination of the elastic field of an ellipsoidal inclusion, and related problems", *Proc. R. Soc. Lond. A. Math. Phys. Sci.* **241** (1957), p. 376-396.
- [40] T. Mori, K. Tanaka, "Average stress in matrix and average elastic energy of materials with misfitting inclusions", *Acta Metall.* **21** (1973), no. 5, p. 571-574.
- [41] C. Pacoste, A. Eriksson, "Beam elements in instability problems", *Comput. Methods Appl. Mech. Eng.* **144** (1997), p. 163-197.
- [42] C. A. Almeida, J. C. R. Albino, I. F. M. Menezes *et al.*, "Geometric nonlinear analyses of functionally graded beams using a tailored Lagrangian formulation", *Mech. Res. Commun.* **38** (2011), p. 553-559.
- [43] D. K. Nguyen, T. T. H. Bui, T. T. H. Tran, S. Alexandrov, "Large deflections of functionally graded sandwich beams with influence of homogenization schemes", *Arch. Appl. Mech.* **92** (2022), p. 1757-1775.
- [44] D. K. Nguyen, "Post-buckling behavior of beams on two-parameter elastic foundation", *Int. J. Struct. Stab. Dyn.* **4** (2004), p. 21-43.
- [45] M. A. Crisfield, *Non-linear Finite Element Analysis of Solids and Structures. Vol 1: Essentials*, Wiley, Chichester, 1991.
- [46] Y. A. Kang, X. F. Li, "Large deflections of a non-linear cantilever functionally graded beam", *J. Reinf. Plast. Compos.* **29** (2010), p. 1761-1774.
- [47] P. K. Masjedi, A. Maher, P. M. Weaver, "Large deflection of functionally graded porous beams based on a geometrically exact theory with a fully intrinsic formulation", *Appl. Math. Model.* **76** (2019), p. 938-957.